Beamstrahlung backgrounds in ILD at linear (ILC) and circular (FCCee) colliders *

Daniel Jeans[1,**]

[1]KEK, Tsukuba, Japan

Abstract. We describe a simulation study of backgrounds in the Time Projection Chamber of the International Large Detector due to beamstrahlung, comparing FCC-ee operating at 91 and 240 GeV with ILC at 250 GeV. This background depends on the amount of initial beamstrahlung per bunch crossing, the design of the machine-detector interface, and the collision rate, which are all significantly different at these different colliders. We also estimate the density of the ion cloud which builds up in the TPC due to this background source.

1 Introduction

The International Large Detector concept (ILD) [1] was originally designed to measure the results of electron positron collisions at the International Linear Collider (ILC) [2] at centre-of-mass energies between 91 GeV and 1 TeV. In recent years several other Higgs Factory electron-positron collider concepts have been proposed. Circular electorn-positron colliders present several important differences compared to linear colliders such as the ILC. The ILD group is currently studying what changes to its baseline detector model would be required to operate at a circular Higgs Factory such as the electron-positron stage of the Future Circular Collider (FCC-ee) [4].

A defining feature of the current ILD design is the large Time Projection Chamber (TPC) [3] which acts as the central component of the tracking system. The ILC provides a relatively benign environment for a TPC, with rather low event rates and occupancies and long quiet periods between "trains" of bunch collisions. The time structure of collisions at a circular collider is very different, with almost continuous collisions.

Could a TPC also operate at a circular Higgs Factory collider such as FCC-ee?

This paper discusses various aspects which could affect the answer to this question, taking the FCC-ee as a concrete example. In particular, backgrounds in the TPC induced by beamstrahlung are investigated. FCC-ee is designed to have less focused beams than ILC, so less beamstrahlung per bunch crossing (BX) is expected. On the other hand, the design of the Machine Detector Interface (MDI) is quite different, with FCC-ee accelerator elements placed much closer to the Interaction Point (IP), so a larger fraction of beamstrahlung particles which scatter into the detector may be expected. In addition, the collision rate at FCC-ee will be much higher than at ILC. The experiment's magnetic field is restricted to 2 T at FCC-ee (at least when running at 91 GeV), which may also increase the effect of such backgrounds.

*This work was carried out in the framework of the ILD concept group

**e-mail: daniel.jeans@kek.jp

2 Beamstrahlung pair backgrounds

Beamstrahlung occurs when beam bunches pass through each other, and beam particles interact with the strong electromagnetic field of the opposing bunch. This produces copious pairs of low p_T electrons and positrons from the conversion of radiated photons. These can produce background hits in the detector either directly, in the case of particles with sufficient p_T to reach the detectors, or indirectly by "splash-back" from interactions of these particles with detector and beamline elements in the forward region. These mostly very low momentum particles essentially curl tightly around the field lines of the experiment's solenoid field.

The simulation of the beamstrahlung process was performed using `GuineaPig` [5] (GP), assuming 250 GeV collisions at ILC with the updated (2017) beam parameters [6], and also for FCC-ee operating at 91 and 240 GeV.

3 Difference in MDI systems at FCC-ee and ILC

The Machine Detector Interface is quite different at FCC-ee and ILC, due to different requirements imposed by collider operation.

- The crossing angle is 30 mrad at FCC-ee, 14 mrad at ILC.
- At ILC the final focus quadruples are placed outside the central detector volume at L*=4.1 m, as are the forward calorimeters such as the luminosity monitor LumiCal (at z ~240 cm). At FCC-ee final focus is closer to the interaction point (L*=2 m), and the LumiCal is positioned at $z \sim 100$ cm.
- At ILC, almost complete calorimetric coverage is envisaged, with space left only for the in– and out–going beampipes. The most significant obstacle to beamstrahlung pairs departing from the detector is the BeamCal, which covers polar angles 5–40 mrad around the outgoing beampipes, at $|z| \sim 3.2$ m. The front face of the BeamCal is covered by 8 cm of graphite to partially absorb low energy backscattered particles. At FCC-ee, the regions with polar angle smaller than 100 mrad are occupied by the MDI system, and are therefore uninstrumented, with the exception of the LumiCal.
- FCC-ee includes tungsten and tantalum shielding around the beampipe to protect the detector and magnets against synchrotron radiation. This is much less of an issue at linear colliders.
- The strength of the experiment's solenoidal magnetic field is limited to 2 T at FCC-ee to preserve beam quality, while at ILC a 3.5 T field is planned.
- The FCC-ee MDI incorporates shielding and compensating solenoids which screen the final focus quadrupoles from the experiment's solenoid field and ensure that zero integrated field is experienced by the beam between the entrance and exit quadrupoles.
- ILD considers the option to include an "anti-DID" field, which adds a small x-component to the B-field in the central detector region to bend the field lines – and therefore the majority of beamstrahlung particles – into the outgoing beampipe.

Since beamstrahlung background in the central detector region is largely caused by splash-back of low momentum particles from the forward region, the description of detector and accelerator materials and fields in the forward region can have a significant influence on the predicted level of such backgrounds.

4 Simulation setup

The detector concept models for ILC and FCC-ee are described using the DD4hep geometry package [7], and are available in [8]. The TPC of ILD is modeled as a cylinder of an Ar-based gas mixture, separated by a central cathode and encased in material corresponding to the field cage and readout infrastructure. The Vertex detector is made up of three double layers of sensitive silicon sensors, with additional material to describe the contribution of support and services. Different vertex geometries geometries are used for ILC–based and FCC-ee–based detectors, due to different beampipe designs in the two MDI systems. Key differences between the models used in this study are summarised in Table 1.

model	B-field [T]	MDI
ILD_l5_v02	3.5 (uniform)	ILC
ILD_l5_v02_2T	2.0 (uniform)	ILC
ILD_l5_v03	3.5 (map)	ILC
ILD_l5_v05	3.5 (map, anti-DID)	ILC
ILD_l5_v11β	2.0 (uniform)	FCC-ee
ILD_l5_v11γ	2.0 (map)	FCC-ee

Table 1. Summary of the detector models used in this study.

The models for the ILC (ILD_l5_v02, v02_2T, v03, v05) have identical material, but differ their magnetic field. For the first two models uniform fields of 3.5 / 2.0 T were used within the volume encased by the solenoid, while the two others use detailed B-field maps resulting from magnetic simulations of the magnet system, with and without an anti-DID field [9].

Models ILD_l5_v11β, γ are test models: they are not fully optimised detector designs but represent an attempt to include the elements required to make reliable estimates of beamstrahlung background rates. Model ILD_l5_v11β is modified from ILD_l5_v02 for use at FCC-ee, with the FCC-ee MDI and a uniform 2 T field. The inner tracking region and forward calorimetry are rather different to the ILC models to accommodate the MDI system, and are adapted from the implemetation developed for the CLD detector model CLD_o2_v05 [8]. Other parts of the detector (TPC, main calorimeters) are identical to ILD_l5_v02. Model ILD_l5_v11γ contains the same material as ILD_l5_v11β, but includes a detailed map of the magnetic field in the central region. Scans of the material and magnetic fields of ILD model variants for use at ILC and FCC-ee are shown in Figs. 1-4.

The ddsim utility was used to simulate the passage of the electrons and positrons given by GuineaPig through the detector model, making use of DD4hep's interface to `Geant4` (G4). G4 steps of ionising particles in the TPC gas volume are collected to produce hits. The readout is radially segmented into volumes representing 220 pad–rows. To ensure that low energy beamstrahlung particles were accurately tracked in the beam vacuum, the maximum step length for electrons and positrons within the beampipe volume was reduced to 10 mm.

The simulated endpoints of MC particles created in the event simulations can help to understand how the beamstrahlung particles interact with the detector material. Fig. 5 shows the position of all such endpoints for 100 BX of beamstrahlung at ILC-250, simulated in all considered detector models. The interaction of the beamstrahlung particles with MDI elements is clearly seen, and is particularly large in the case of the ILD_l5_v11 models.

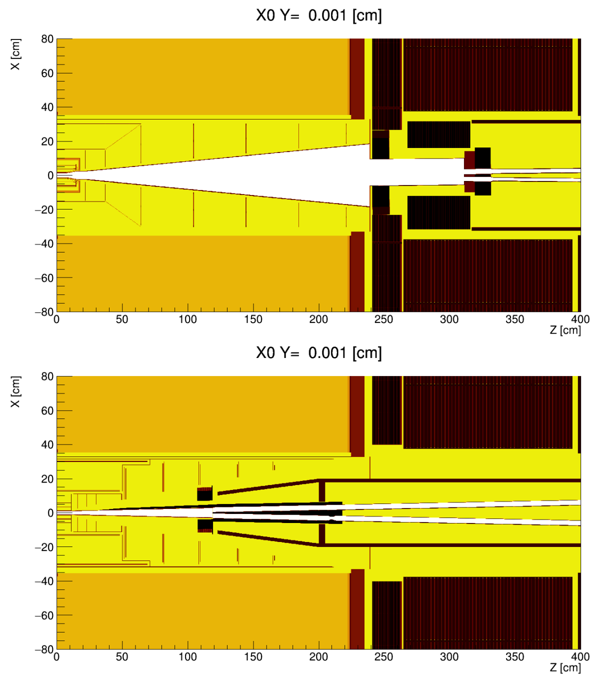

Figure 1. Detector models used in this study. The top figure shows the "standard" geometry at ILC (ILD_l5_v02), and the lower one shows the design adopted for use at FCC-ee (ILD_l5_v11γ). Darker colours show material with shorter radiation length. The orange region at $|X| > 35$ cm, $Z < 220$ cm is the inner part of the TPC gas volume.

5 TPC results

Figure 6 shows the distribution of ions generated in the TPC, integrated over 100 bunch crossings of FCC-91 in the ILD_l5_v11γ detector model, and of ILC-250 for the ILD_l5_v03 detector model. Most hits are produced by "micro-curlers", very low energy electrons produced in the TPC gas which spiral along the field lines. The number of hits is visibly larger in the case of ILC-250, and the hit density is larger at small radii.

The MC particles associated to the TPC hits can help understand the origin of hits in the TPC. For each TPC hit, the MC history of the particle which created it is traced back to the original electron/positron ancestor from GuineaPig. Distributions of these original GuineaPig particles which go on induce TPC hits are shown in Fig. 7 for different collider/detector combinations.

Each hit's oldest MC ancestor which was created in the Geant4 simulation was also identified (i.e. the ancestor coming immediately after the original electron/positron from GuineaPig). The z position at which this particle was created is shown in Fig. 8 for the case of the ILD_l5_v11γ detector model at FCC-91.

A strong contribution is seen at $|z| \sim 1200$ mm; comparing to Fig. 1, this appears to be due to the shielding around the position at which the two beampipes merge, which is indeed the first material seen by particles traveling along the detector axis.

Around 87% of TPC hits are linked to photons in their MC history. Figure 9 shows, for TPC hits with a photon in their ancestry, the position at the hit's direct ancestor was created. This direct ancestor may be the photon itself, or the last descendant of the photon. Also shown

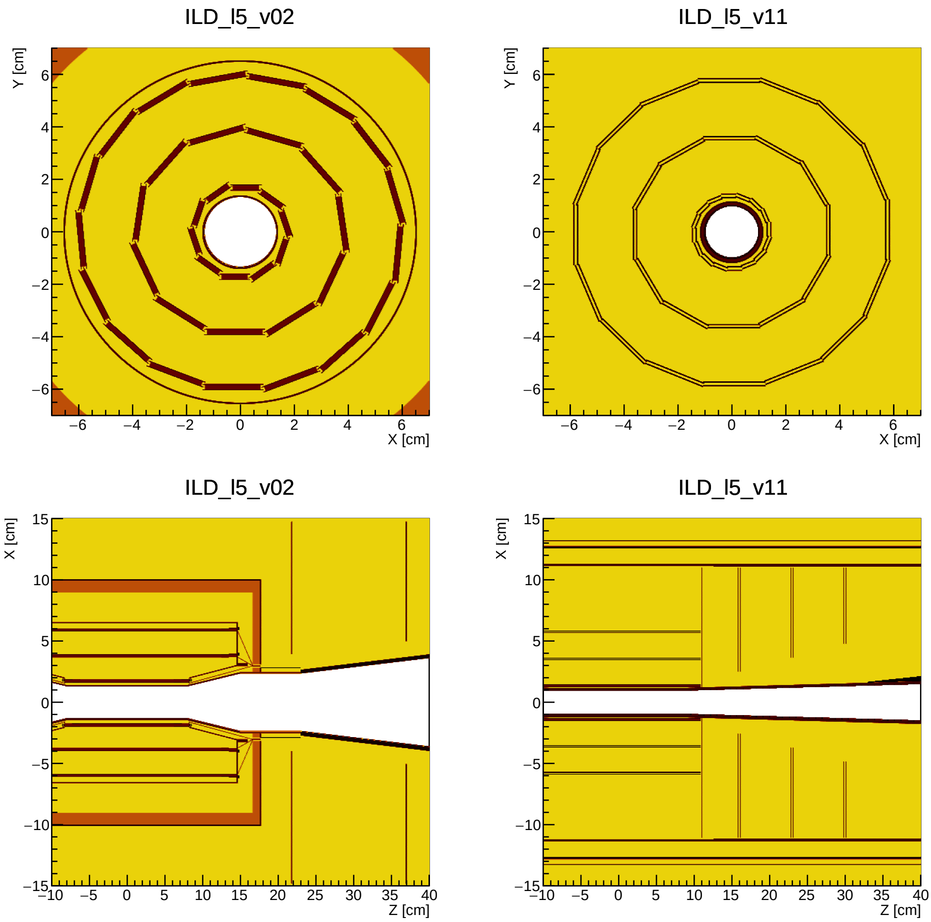

Figure 2. Vertex detector layout in the ILD variants for the ILC (left) and the CLD-inspired design for FCC (right).

is the energy distribution of the photons ancestor. These TPC hits are typicallt induced by particles created in the inner part of the detector, within a few cm of the beamline. The distribution in z shows contributions from various elements of the MDI. The typical energy of photons which induce TPC hits is in the MeV range.

5.1 Numerical results

To estimate the number of primary ions produced in each TPC hit, the deposited energy associated to the hit is divided by the effective ionisation energy of Argon, 26 eV. The number of ions per bunch-crossing (BX) is obtained by summing over all hits in a single bunch-crossing. Since this number can vary significantly between BXs, an average is taken over a sample of 100 BX. The resulting average number of primary ions produced in the TPC volume per BX are presented in Table 2, for a variety of different detector models at ILC and FCC-ee. The RMS of the bunch-by-bunch variation is also shown.

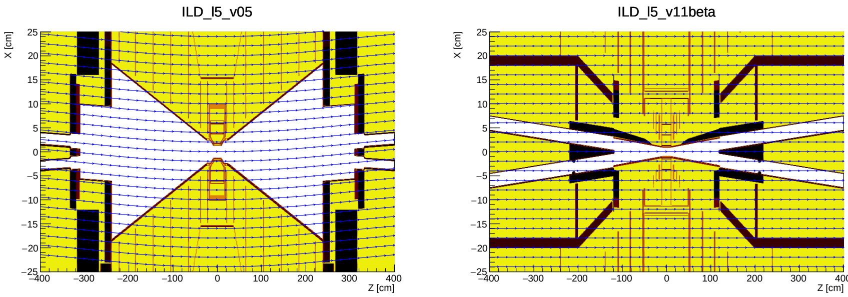

Figure 3. Magnetic field lines in $x - z$ plane at $y = 0$ in the central region of the ILD_l5_v05 (left) and ILD_l5_v11β (right) detector models. Starting at the IP, field lines exit ILD_l5_v05 through the outgoing beampipes, while in the case of ILD_l5_v11β they intersect the masking material at the junction of the two beampipes.

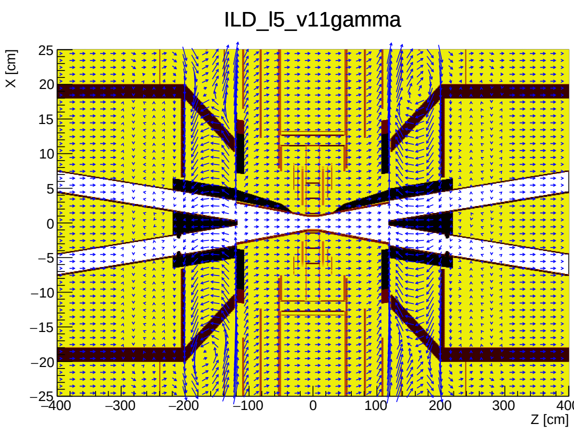

Figure 4. Magnetic field in the $x - z$ plane at $y = 0$ in the central region of the ILD_l5_v11γ detector model, showing the complex field in the region of the screening and compensation solenoids. The direction (length) of arrows represent the orientation (magnitude) of the field's $x - z$ component.

There are very large differences of up to five orders of magnitude in the mean number of primary ions per BX between the different colliders, energies, and detector models. Notable features are:

- **Effect of collider.** Comparing the results of FCC-240 and ILC-250, the ILC bunch crossings induce around 2 orders of magnitude more background hits for a given detector model. Since the ILC bunches are more focused, the beamstrahlung is stronger.
- **Effect of MDI design.** ILD_l5_v02_2T and ILD_l5_v11β use the same field description but different machine elements. ILD_l5_v11β produces TPC backgrounds around two orders larger than at ILD_l5_v02, induced by the presence of more material in the central part of the detector volume.
- **Bunch-to-bunch variation.** The number of primary ions fluctuates significantly from bunch to bunch. For example, 100 BX of FCC-91 were analysed in the ILD_l5_v11γ

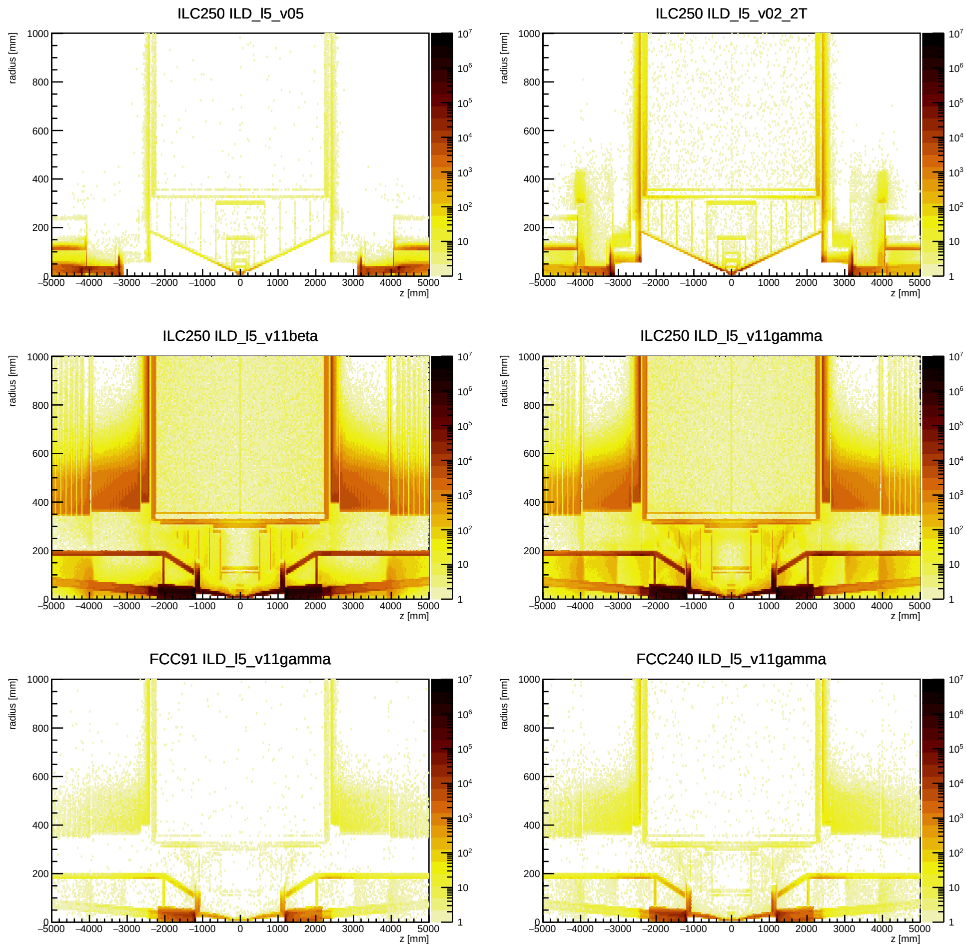

Figure 5. Pair backgrounds at ILC-250, FCC-91 and FCC-240 in different detector models: distribution in radius and z of the endpoint of all MC particles, integrated over 100 BX. Top row: ILC detector variants at ILC-250; middle row: FCC-ee detector variants in the ILC-250 environment (unrealistic, shown for comparison only); bottom row: FCC-ee detector variant at FCC-91/240.

model. The number of primary ions per BX ranges from 120k to 670k, with a mean of 270k, median of 240k, and RMS of 100k.

- **Effect of the magnetic field.** In the case of the ILC-MDI, reducing the uniform magnetic field from 3.5 T to 2.0 T does not significantly change the background for FCC-ee collisions, but results in an increase by a factor 5 at ILC-250, potentially due to the presence of more relatively higher p_T particles at ILC-250.
- **Effect of anti-DID.** Comparing ILD_l5_v03 (no anti-DID) and ILD_l5_v05 (with anti-DID), the inclusion of an anti-DID field reduces TPC backgrounds at ILC-250 by around a factor 2.
- **Effect of BeamCal's graphite layer.** The 8 cm thick graphite layer in front of BeamCal reduces the TPC background by $\sim 20\%$ at ILC-250.

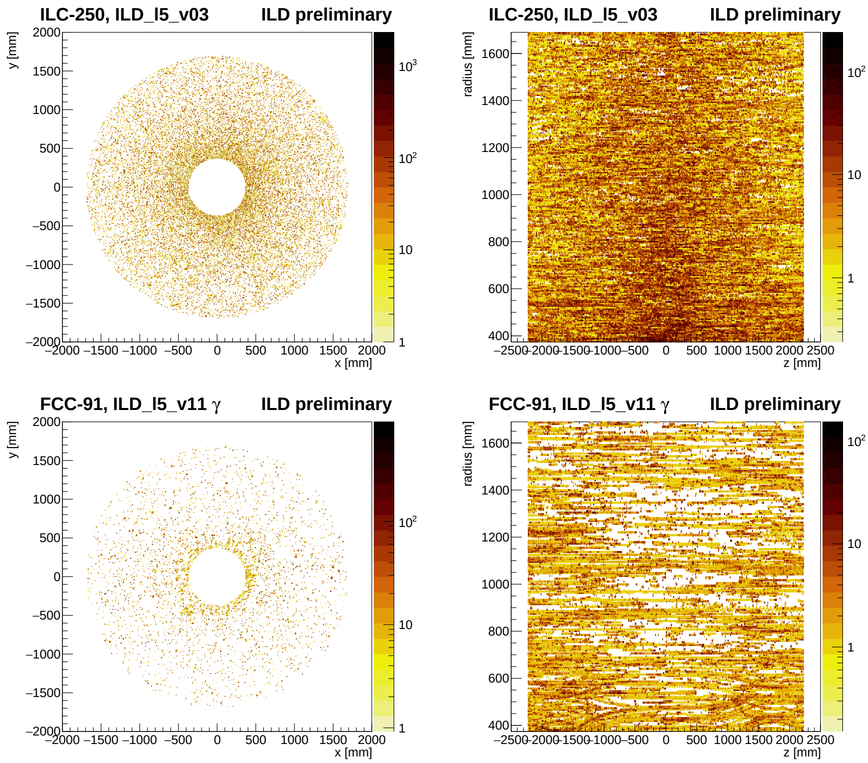

Figure 6. Distribution of TPC hits in (top) ILD_l5_v03 at ILC-250, and (bottom) ILD_l5_v11γ at FCC-91, integrating over 100 bunch crossings. Left: x–y projection, right: z–radius projection.

- **Realistic estimates.** In the case of FCC-ee collisions in ILD_l5_v11γ (i.e. a detector with FCC-ee-MDI and detailed field description), 0.27 (0.8) million primary ions per BX are expected at 91 (240) GeV.

  In the case of a detector model with ILC-MDI at the ILC-250, 0.45 (1.1) million primary ions per BX are expected when using a realistic field map with(-out) an anti-DID field. The number of TPC background hits per BX expected at FCC-ee and ILC-250 is similar when we use the MDI system appropriate for the accelerator.

The radial dependence of the charge density due to primary ions per BX is shown in Fig. 10, showing the significantly larger density at small radii, at larger collision energy, and ant the ILC with its stronger beamstrahlung.

5.2 Ion cloud

The drift speed of ions in the T2K gas and electrical field evisaged for the ILD TPC is around 5 m/s. (The dift speed for electrons is around 7.5 cm/μs, more than 10000 times faster.) The maximum drift length is between the central cathode and readout plane, around 2.2 m, giving a maximum drift time of 0.44 s. At any one time, the TPC therefore contains ions from any collisions which occurred during the previous 0.44 s. The total numbers of ions in the TPC volume at any time therefore depends both on the number ions produced per BX and on the collision frequency.

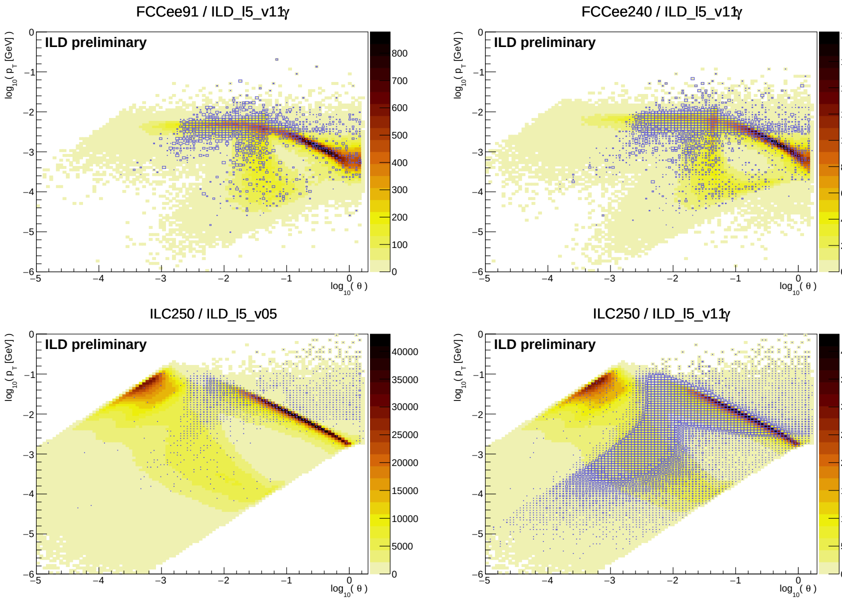

Figure 7. Distribution of beamstrahlung particles in the nominal centre-of-mass frame. The colour scale shows the initial distribution of pair particles and the box histogram shows the distribution of particles which induced hits in the TPC, weighted by the number of TPC hits. The contribution seen in the case of ILC250 at a fraction of a mrad and p_T around 0.1 GeV is due to Compton scattering, which was likely turned off for the GuineaPig simulations of FCC-ee. It has a minimal effect on the TPC backrounds in the case of ILC250, so it is reasonable to assume that the same will be true at FCC-ee and that it can be safely ignored for the purposes of the present study.

At FCC-91, the 30 MHz collision frequency is three orders of magnitude larger than the average at ILC; at FCC-240 it is two orders of magnitude larger. The number of BXs which contribute to the TPC's ion cloud is 13.2 M, 325 k, and 2.9 k respectively at FCC-91, FCC-240, and ILC-250.

A rough estimate of the number of primary ions present in the TPC at any one time is (maximum drift time = 0.44 s) × (BX frequency [Hz]) × (ions produced / BX) × 0.5, where the final factor accounts for the fraction of ions produced in previous BXs which have already arrived at (and been neutralised by) the cathode. Considering that the volume of the ILD-TPC is around 42 m^3 one can estimate the average charge density in the TPC volume, as shown in Table 3. The ion density will vary throughout the TPC volume, with dependence on radius and z, but here only the average density is considered. The charge density of 6.8 nC/m^3 (0.54 nC/m^3) estimated at FCC-91 (FCC-240) is 2500 (200) times larger than at ILC-250.

Significant additional contribution to the ion cloud is expected due to secondary ions produced by gas amplification in the readout modules. Thanks to the bunch train structure at ILC, a gating device can be used. This uses electric fields to prevent particles passing between the amplification device and the main TPC volume, except during the time at which ionisation electrons, whose drift speed is several orders of magnitude faster than that of ions, are expected to arrive. Such a gate can block the vast majority of secondary ions, preventing them from reaching the main gas volume. The small fraction of secondary ions that do pass the gate form disks (one per bunch train) which sweep through the TPC volume. When ILC operates at 5 Hz, up to three such disks are present in each half of the TPC.

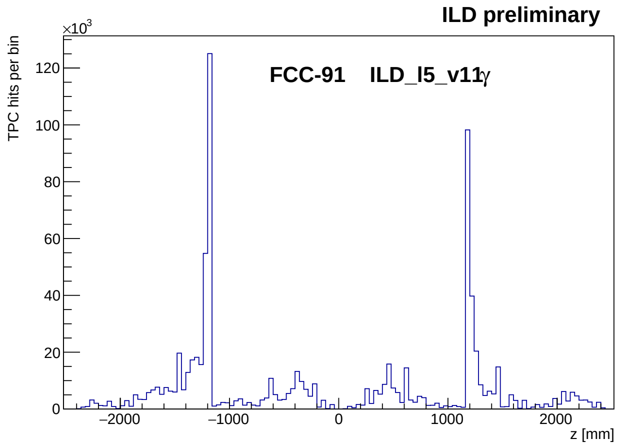

Figure 8. Distribution in z of the position of the first simulated interaction which gave rise to a TPC hit. ILD_l5_v11γ detector model, 100 BX of pair background at FCC-91.

			FCC-91	FCC-240	ILC-250
		bunch crossing frequency	30 MHz	800 kHz	6.6 kHz
model	B-field [T]	MDI	thousand ions / bunch crossing mean ± RMS		
ILD_l5_v02	3.5 (uniform)	ILC	6.5 ± 19.9	14 ± 14	960 ± 150
ILD_l5_v02_2T	2.0 (uniform)	ILC	6.9 ± 11.1	15 ± 11	4700 ± 300
ILD_l5_v03	3.5 (map)	ILC	5.7 ± 7.9	14 ± 11	1100 ± 200
ILD_l5_v05	3.5 (map, anti-DID)	ILC	0.6 ± 1.5	3.7 ± 9.7	450 ± 110
ILD_l5_v11β	2.0 (uniform)	FCC-ee	390 ± 120	1000 ± 170	110000 ± 2400
ILD_l5_v11γ	2.0 (map)	FCC-ee	270 ± 100	800 ± 140	100000 ± 1900
removing BeamCal's graphite layer					
ILD_l5_v03	3.5 (map)	ILC			1300 ± 170
ILD_l5_v05	3.5 (map, anti-DID)	ILC			590 ± 120

Table 2. Mean and RMS of the number of primary ions produced by beamstrahlung background in the TPC per bunch crossing in various collider and detector configurations.

The quasi-continuous collisions at FCC-ee preclude the use of a similar gating device, since the signal ionisation electrons are continuously arriving at the TPC readout plane. Novel approaches to the blocking of secondary ions are therefore needed in the FCC-ee environment.

We can compare these charge densities to those experienced in the TPC of the ALICE experiment, where a charge density varying with radius between 20 and 120 fC/cm^3 ≡ nC/m^3 is expected, giving rise to distortions of several cm [10]. This includes a dominant contribution from secondary ions produced in the gas amplification. The maximum *primary* ion cloud density we esimate at FCC-91 is around 4 times smaller than the maximum expected at ALICE. Once the effects of secondary ions at FCC-91 are included, a rather similar density is expected.

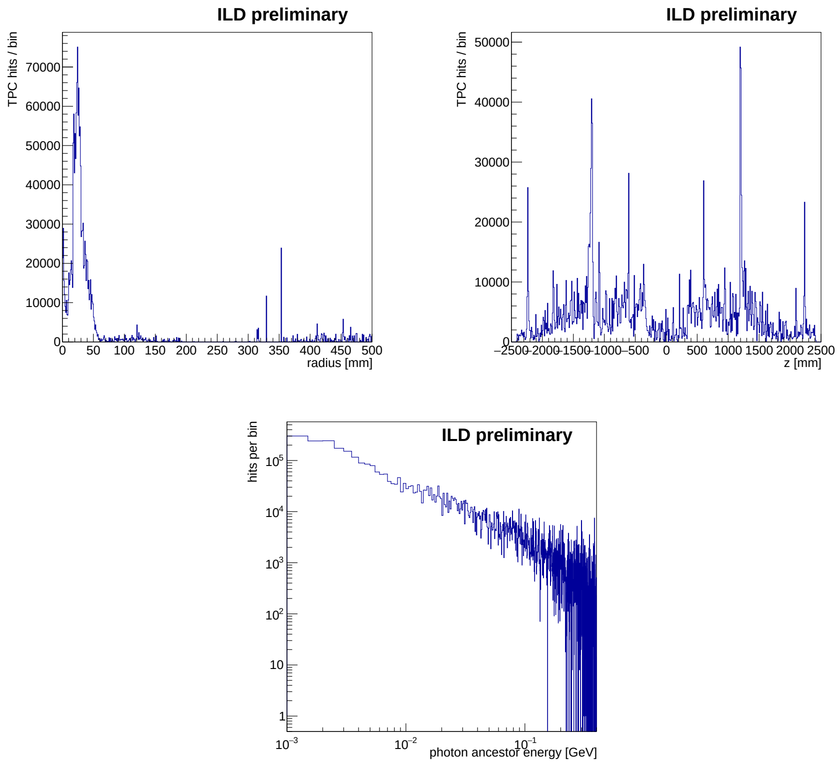

Figure 9. Properties of TPC hits created directly or indirectly by photons, for the ILD_l5_v11γ model operating at FCC-240. Top: distributions in radius and z of the point at which TPC hits' immediate parent was created; Bottom: the energy of hits' photon ancestor.

Collider Detector model	FCC-91 ILD_l5_v11γ	FCC-240 ILD_l5_v11γ	ILC-250 ILD_l5_v05
average BX frequency	30 MHz	800 kHz	6.6 kHz
primary ions / BX	270 k	800 k	450 k
primary ions in TPC at any time	1.8×10^{12}	1.4×10^{11}	6.5×10^{8}
average primary ion charge density nC/m^3	6.8	0.54	0.0025

Table 3. Rough estimates of the average ion cloud within the TPC at different colliders.

5.3 Other TPC background sources

So far, only the effect of beamstrahlung has been considered. Particularly when running a circular collider at 91 GeV, the rate of high multiplicity physics events $e^+e^- \to q\bar{q}$ is extremely high due to the very large cross-section ($\sim$ 30 nb) and luminosity (2×10^{34}cm^{-2}s^{-1}), giving a rate of such hadronic events of around 60 kHz at FCC-91. A full simulation of this process suggests that each such event produces on average around 1 million primary ions within the TPC. We estimate that this will give rise to around $0.44[\mathrm{s}]\times 60\cdot 10^3[\mathrm{Hz}]\times 1\cdot 10^6[\mathrm{ions/event}]\times 0.5 = 1.3\cdot 10^{10}$ primary ions in the TPC at any time, two orders of magnitude less than the contribution from beamstrahlung.

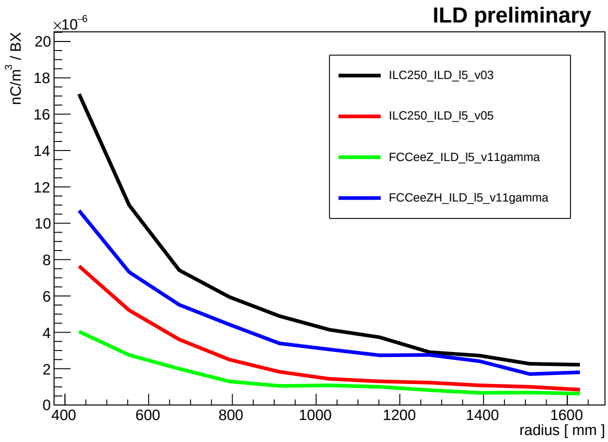

Figure 10. Radial dependence of the primary ion charge density induced by beamstrahlung in a single BX in the realistic collider/detector combinations.

A previous study for CEPC [11] considered the effect of the ions from this source, and concluded that a TPC can be used at a circular collider operating at the Z-pole provided that ion back-flow is well controlled, and raised the point that significant distortions of electron trajectories will be induced by the ion cloud. However, according to the present study, this contribution from $e^+e^- \to q\bar{q}$ represents less than 1% of the ions produced by beamstrahlung at FCC-91.

5.4 Mitigation strategies?

The main tool to try to reduce the primary ion density in the TPC at a circular collider is likely the design of the forward shielding in the FCC-ee MDI. Since this shielding plays an essential role in the reduction of synchrotron radiation-related detector backgrounds, it is probably not feasible to significantly reduce it. Could the geometry be adjusted to a more “stealthy” design, which deflects backgrounds into less important regions?

It may be possible to include including additional shielding to reduce or absorb splash-back from these masks. A system similar to the graphite absorber placed in front of the BeamCal at ILC, which reduces TPC ions from beamstrahlung background by around 20%, is not likely to be sufficient: a more massive shield would probably be required to shield the TPC from the MeV-scale photons back-splashing from the MDI elements.

A change in TPC gas and/or applied electric field to increase the ion drift speed may also be a means of reducing the ion clous to some extent.

The magnetic field configuration may also be a useful tool to steer the low p_T pairs out of the detector rather than into MDI elements, similarly to the anti-DID field at ILC. However the field design at FCC-ee is already rather complex to satisfy the stringent constraints coming from the accelerator, and it is not clear to the author how much freedom there is to adjust the field.

Sophisticated AI-based strategies have been developed to correct for space-charge distortions in the ALICE TPC [12]. Similar approaches applied at a circular electron-positron collider may go some way towards maintaining the TPC spatial resolution required for the physics program at such a facility. The use of a TPC with pixel-based readout may help with this type of approach.

6 Conclusion

Operating the ILD at a circular collider will likely require some changes to the baseline design to deal with the different experimental environment. We have presented a study of the effects of beamstrahlung backgrounds on ILD's time projection chamber, comparing the situation at ILC-250, FCC-91 and FCC-240.

The situation of the TPC is challenging due to the long time needed to clear the ions from the gas volume. The primary ion density in the TPC gas volume is likely to be more than five orders of magnitude larger at FCC-91 than at ILC-250, due to a combination of the MDI design ($\sim$ 2 orders) and the collision frequency ($\sim$ 3 orders). If the quasi-continuous collisions at FCC-ee make it more difficult to block secondary ions from the readout gas amplification, this could add further factors.

Acknowledgments

Particular thanks are due to to A. Ciarma (CERN) and colleagues for providing samples of pair background data at FCC-ee and the FCC-ee MDI field map, as well as to ILD colleagues for several stimulating discussions and suggestions.

References

[1] H. Abramowicz et al. [ILD Concept Group], *International Large Detector: Interim Design Report*. arXiv:2003.01116 (2020)

[2] T. Behnke et al., *The International Linear Collider Technical Design Report - Volume 1: Executive Summary*. arXiv:1306.6327 (2013)

[3] J. Kaminski [LCTPC], *TPC development by the LCTPC collaboration for the ILD detector at ILC*. J. Phys. Conf. Ser. **2374**, no.1, 012149 (2022), arXiv:2203.03435

[4] A. Abada et al. [FCC], *FCC-ee: The Lepton Collider: Future Circular Collider Conceptual Design Report Volume 2*. Eur. Phys. J. ST **228**, no. 2, 261-623 (2019)

[5] D. Schulte, *Study of Electromagnetic and Hadronic Background in the Interaction Region of the TESLA Collider*. PhD thesis, DESY (1997)

[6] L. Evans, S. Michizono, *The International Linear Collider Machine Staging Report 2017*. arXiv:1711.00568 (2017)

[7] https://dd4hep.web.cern.ch/dd4hep (2024)

[8] https://github.com/key4hep/k4geo (2024)

[9] U. Schneekloth, *ILD Solenoid Field Simulations*. https://agenda.linearcollider.org/event/7350/contributions/37271/ (2016)

[10] ALICE collaboration, *Upgrade of the ALICE Time Projection Chamber*. CERN-LHCC-2013-020 (2013)

[11] M. Zhao et al., *Feasibility study of TPC at electron positron colliders at Z pole operation*. JINST **12**, no.07, P07005 (2017) arXiv:1704.04401

[12] S. Gorbunov et al., *Deep neural network techniques in the calibration of space-charge distortion fluctuations for the ALICE TPC*. EPJ Web of Conferences **251**, 03020 (2021)

[13] Y. Bilevych et al., *Status Pixel TPC R&D*. https://agenda.linearcollider.org/event/10211/contributions/53826/ (2024)